[3] H Abe, "A GaAs MESFET oscillator quasi-linear design method," *IEEE Trans. Microwave Theory Tech*, vol MTT-34, pp. 19–25, Jan 1986.
[4] Y. Xuan and C. M Snowden, "A generalized approach to the design of microwave oscillators," *IEEE Trans Microwave Theory Tech.*, vol. MTT-35, pp 1340–1347, Dec. 1987.
[5] R. S. Pengelly, *Microwave Field-Effect Transistors: Theory, Design and Applications*, 2nd ed. Letchworth, England: Research Studies Press, 1986.

An Analytical Two-Dimensional Perturbation Method to Model Submicron GaAs MESFET's

E DONKOR, MEMBER, IEEE, AND
F. C. JAIN, SENIOR MEMBER, IEEE

Abstract — **A two-dimensional analytical model has been developed for the potential distribution in submicron GaAs MESFET's. The potential distribution is obtained by solving Poisson's equation with nonrectangular boundary conditions using a perturbation method. The expression for the potential is used to derive the current–voltage relation for GaAs MESFET's having channel lengths ranging from 0.2 to 0.9 μm. The model is applicable in the linear, the saturation, and the subthreshold regimes of the current–voltage characteristics. Numerically simulated results are compared with experimental data and are found to be in good agreement.**

I. Introduction

Gallium arsenide (GaAs) FET's used in high-performance microwave and millimeter-wave circuits increasingly require submicron feature sizes [1], [2]. The electrical characteristics of these scaled-down devices are known to be greatly influenced by the two-dimensional potential distribution and high electric field effects [3]–[5].

Analytical models based on the one-dimensional gradual channel approximation method [6] do not adequately account for these effects. The dependence of the electrical characteristics on the electric field near the drain end has been recognized by many authors, including Dacey and Ross [7], Pucel and Haus [8], Yamaguchi *et al.* [9], and Fair [10]. Recently, Meindl and Marshall [11] proposed a two-dimensional model for characterizing the subthreshold operation of Si MESFET's. Kimiyoshi and Masahiro [12] have also presented a two-dimensional model to predict the current–voltage relation in the saturation region of GaAs MESFET's. Most of the models reported in the literature are applicable in a limited region, such as the saturation or subthreshold region. In this paper a two-dimensional analytical model, accounting for high electric field and two-dimensional effects, is presented to characterize the electrical behavior of submicron GaAs MESFET's. The model is applicable in the subthreshold, the linear, and to some degree the saturation regimes. In addition, it is useful for both normally off and normally on devices.

II. Theory

The approach is based on the determination of the two-dimensional potential distribution in the depletion region under the Schottky gate of a MESFET. The formulation is presented in this section and details are described in Section III. The potential is then used to derive the current–voltage relation in the channel. This is treated in Section IV.

Manuscript received January 8, 1989; revised April 13, 1989. This work was supported by a grant from the Connecticut Department of Higher Education
The authors are with the Microelectronics Research Laboratory, Electrical and Systems Engineering Department, University of Connecticut, Storrs, CT 06269-3157.
IEEE Log Number 8929185.

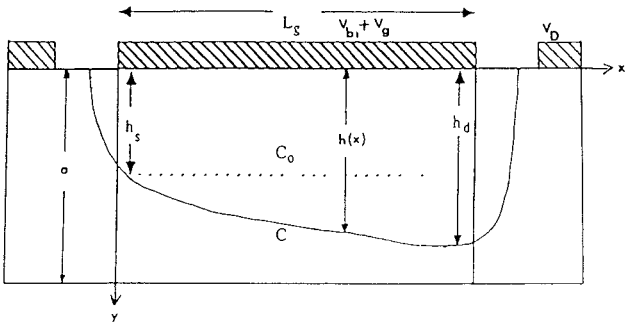

Fig. 1. Simplified GaAs MESFET geometry

The total electrostatic potential in the depletion region under the gate $\phi(x, y)$ is obtained by solving the Poisson equation using appropriate boundary conditions. The Poisson equation is given by

$$\frac{\partial^2\phi(x,y)}{\partial x^2}+\frac{\partial^2\phi(x,y)}{\partial y^2}=-\frac{qN_D}{\epsilon}. \tag{1}$$

Here N_D is the doping concentration (assumed to be uniform), q is the electronic charge, and ϵ is the permittivity. Following the approach in [11], the potential $\phi(x, y)$ in (1) above is expressed as a superposition of two functions, $U(x, y)$ and $\psi(x, y)$, such that

$$\phi(x,y)=U(x,y)+\psi(x,y) \tag{2}$$

where the functions $U(x, y)$ and $\psi(x, y)$ satisfy the following equations:

$$\frac{\partial^2\psi(x,y)}{\partial x^2}+\frac{\partial^2\psi(x,y)}{\partial y^2}=0 \tag{3}$$

$$\frac{\partial^2U(x,y)}{\partial x^2}+\frac{\partial^2U(x,y)}{\partial y^2}=-\frac{qN_D}{\epsilon}. \tag{4}$$

The solution to (3) is obtained using the perturbation method [13]. The perturbation method involves the solution of a set of Laplace equations in the rectangular region bounded by C_0 (see Fig. 1). The actual potential $\psi(x, y)$ in the nonrectangular region bounded by C is then expressed in terms of ψ_0, ψ_1, and higher order components using a perturbation parameter λ $(0<\lambda<1)$. An assumed solution is of the form

$$\psi=\psi_0+\lambda\psi_1+\lambda^2\psi_2+\lambda^3\psi_3+\cdots. \tag{5}$$

The substitution of (5) into (3) results in a sequence of Laplace equations involving the ψ's. The condition at the lower boundary for the Laplace equations in terms of ψ_0, ψ_1, ψ_2, etc., is determined by relating the conditions on the actual boundary C (see Fig. 1) to C_0 of the hypothetical rectangle. The other boundary conditions for the ψ's require an expression for $U(x, y)$. This is obtained from the solution of (4) assuming significant variations along the y axis. Since the field $\partial\psi(x, y)/\partial y$ approaches zero at the depletion edge, neglecting the x variation in the boundary C would not cause significant error. The solution involves integrating (4) twice with respect to y and using appropriate boundary

0018-9480/89/0900-1484$01.00 ©1989 IEEE

conditions. This results in

$$U(x,y) = V_{bi} + V_g + qN_D y \frac{(2h(x) - y)}{2\epsilon} \tag{6}$$

where V_{bi} is the built-in voltage and V_g is the gate voltage.

Details of the perturbation approach are given below.

III. Evaluation of the Potential $\psi(x, y)$

In most FET analyses, the depletion edge boundary is invariably replaced [9], [11] by the total channel depth. However, the perturbation method allows the solution of the Laplace equation using the nonrectangular boundary C representing the depletion edge. The Laplace equations for the ψ's are obtained by substituting (5) into (3) to get

$$0 = \frac{\partial^2}{\partial x^2}(\psi_0 + \lambda\psi_1 + \lambda^2\psi_2 + \lambda^3\psi_3 + \cdots) + \frac{\partial^2}{\partial y^2}(\psi_0 + \lambda\psi_1 + \lambda^2\psi_2 + \lambda^3\psi_3 + \cdots). \tag{7}$$

Regroup the terms in the above equation as follows:

$$0 = \left\{\frac{\partial^2\psi_0}{\partial x^2} + \frac{\partial^2\psi_0}{\partial y^2}\right\} + \lambda\left\{\frac{\partial^2\psi_1}{\partial x^2} + \frac{\partial^2\psi_1}{\partial y^2}\right\} + \lambda^2\left\{\frac{\partial^2\psi_2}{\partial x^2} + \frac{\partial^2\psi_2}{\partial y^2}\right\} + \lambda^3\left\{\frac{\partial^2\psi_3}{\partial x^2} + \frac{\partial^2\psi_3}{\partial y^2}\right\} + \lambda^4\left\{\frac{\partial^2\psi_4}{\partial x^2} + \frac{\partial^2\psi_4}{\partial y^2}\right\} + \cdots. \tag{8}$$

Since λ is nonzero, the above equation leads to the following sequence of Laplace equations:

$$\frac{\partial^2\psi_0}{\partial x^2} + \frac{\partial^2\psi_0}{\partial y^2} = 0 \qquad \text{for } \lambda^0 \tag{9}$$

$$\frac{\partial^2\psi_1}{\partial x^2} + \frac{\partial^2\psi_1}{\partial y^2} = 0 \qquad \text{for } \lambda^1. \tag{10}$$

Next, determine the boundary conditions for the Laplace equations. To do this notice that each point on C can be obtained by an outward normal displacement of points on C_0. Let each point on C_0 be displaced along the outward normal by an amount $\lambda h(x)$. Then the condition $\partial\psi/\partial y = 0$ on C becomes

$$0 = \left.\frac{\partial\psi}{\partial y}\right|_{C_0} + \lambda h(x)\left.\frac{\partial^2\psi}{\partial y^2}\right|_{C_0} + \frac{\lambda^2 h^2(x)}{2!}\left.\frac{\partial^3\psi}{\partial y^3}\right|_{C_0} + \frac{\lambda^3 h^3(x)}{3!}\left.\frac{\partial^4\psi}{\partial y^4}\right|_{C_0} + \cdots. \tag{11}$$

Next substitute (5) into (11) to get

$$0 = \frac{\partial}{\partial y}(\psi_0 + \lambda\psi_1 + \lambda^2\psi_2 + \cdots)\Big|_{C_0} + \lambda h(x)\frac{\partial^2}{\partial y^2}(\psi_0 + \lambda\psi_1 + \lambda^2\psi_2 + \cdots)\Big|_{C_0} + \frac{\lambda^2 h^2(x)}{2!}\frac{\partial^3}{\partial y^3}(\psi_0 + \lambda\psi_1 + \lambda^2\psi_2 + \cdots)\Big|_{C_0} + \frac{\lambda^3 h^3(x)}{3!}\frac{\partial^4}{\partial y^4}(\psi_0 + \lambda\psi_1 + \lambda^2\psi_2 + \cdots)\Big|_{C_0} + \cdots. \tag{12}$$

Equation (12) leads to the following sequence of boundary conditions:

$$\left.\frac{\partial\psi_0}{\partial y}\right|_{C_0} = 0 \qquad \text{for } \lambda^0 \tag{13}$$

$$\left.\frac{\partial\psi_1}{\partial y}\right|_{C_0} + h(x)\left.\frac{\partial^2\psi_0}{\partial y^2}\right|_{C_0} = 0 \qquad \text{for } \lambda^1. \tag{14}$$

Thus the Laplace equation with the associated set of boundary conditions for the fundamental potential $\psi_0(x, y)$ and the first harmonic potential $\psi_1(x, y)$ are as follows:

Laplace equation:

$$\frac{\partial^2\psi_0}{\partial x^2} + \frac{\partial^2\psi_0}{\partial y^2} = 0. \tag{15a}$$

Boundary conditions:

$$\psi_0(x,0) = 0 \tag{15b}$$

$$\frac{\partial\psi_0(x,h_s)}{\partial y} = 0 \tag{15c}$$

$$\psi_0(0,y) = -\left[V_{bi} + V_\epsilon + \frac{qN_D y}{2\epsilon}(h_s - y)\right] \tag{15d}$$

$$\psi_0(L_g,y) = V_D - \left[V_{bi} + V_g + \frac{qN_D y}{2\epsilon}(h_d - y)\right]. \tag{15e}$$

Laplace equation:

$$\frac{\partial^2\psi_1}{\partial x^2} + \frac{\partial^2\psi_1}{\partial y^2} = 0. \tag{16a}$$

Boundary conditions:

$$\psi_1(x,0) = 0 \tag{16b}$$

$$\frac{\partial\psi_1(x,h_s)}{\partial y} = -h(x)\frac{\partial\psi_0^2(x,h_s)}{\partial y^2} \tag{16c}$$

$$\psi_1(0,y) = 0 \tag{16d}$$

$$\psi_1(L_g,y) = 0. \tag{16e}$$

The solutions to (15a) and (16a) with the corresponding boundary conditions can be obtained using Fourier series and are given by [14]

$$\psi_0 = \sum_{n=0}^{\infty}\left[A_n \sinh\frac{(2n+1)\pi x}{2h_s} + B_n \sinh\frac{(2n+1)\pi(L_g - x)}{2h_s}\right]\cdot\sin\frac{\pi(2n+1)y}{2h_s} \tag{17}$$

$$\psi_1 = \sum_{n=0}^{\infty} C_n \sin\frac{\pi(2n+1)x}{L_g}\sinh\frac{\pi(2n+1)y}{L_g}. \tag{18}$$

Combining (6), (17), and (18) gives the complete expression for $\phi(x, y)$ as

$$\phi = V_{bi} + V_g + qN_D y\frac{(2h(x) - y)}{2\epsilon} + \sum_{n=0}^{\infty}\left[A_n \sinh\frac{(2n+1)\pi x}{2h_s} + B_n \sinh\frac{(2n+1)\pi(L_g - x)}{2h_s}\right]\cdot\sin\frac{(2n+1)\pi y}{2h_s} + \lambda\sum_{n=0}^{\infty}\left[C_n \sin\frac{\pi(2n+1)x}{L_g}\sinh\frac{(2n+1)\pi y}{L_g}\right] \tag{19}$$

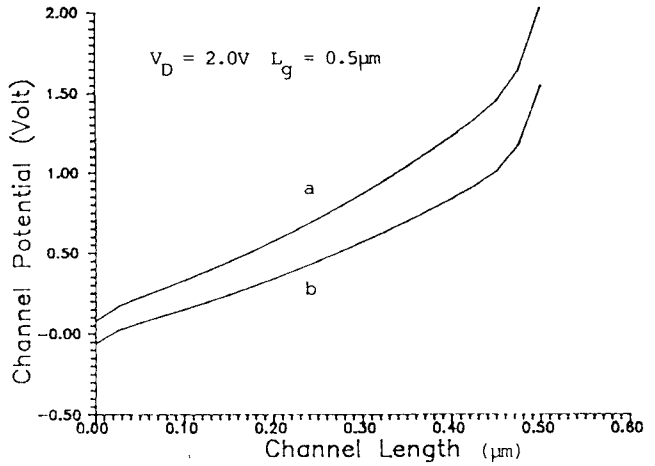

Fig. 2. Channel potential versus channel length. Curve *a*: with perturbation. Curve *b*: without perturbation.

with

$$A_n = \frac{4}{\pi(2n+1)\sinh\dfrac{(2n+1)\pi L_g}{2h_s}} \cdot \left[V_D - \frac{4qN_D h_s h_d}{\epsilon\pi^2(2n+1)^2} - V_{bi} - V_G\right] \tag{20}$$

$$B_n = \frac{-4}{\pi(2n+1)\sinh\dfrac{(2n+1)\pi L_g}{2h_s}} \left[\frac{4qN_D h_s^2}{\epsilon\pi^2(2n+1)^2} + V_{bi} + V_G\right] \tag{21}$$

and also

$$C_n = \frac{2(A_n - B_n)m_0}{L_g \cosh\dfrac{(2n+1)\pi h_s}{L_g}\left\{1+\dfrac{4h_s^2}{L_g^2}\right\}} \sinh\frac{(2n+1)\pi L_g}{2h_s} - \frac{8(A_n - B_n)m_1 h_s}{L_g \cosh\dfrac{(2n+1)\pi h_s}{L_g}\left\{1+\dfrac{4h_s^2}{L_g^2}\right\}^2} \cosh\frac{(2n+1)\pi L_g}{2h_s} + \frac{2A_n m_1}{\cosh\dfrac{(2n+1)\pi h_s}{L_g}\left\{1+\dfrac{4h_s^2}{L_g^2}\right\}^2} \sinh\frac{(2n+1)\pi L_g}{2h_s}. \tag{22}$$

Fig. 2 shows a plot of the potential distribution along the depletion edge boundary C of Fig. 1. Curve b was obtained by neglecting the perturbation (last) term of (19), and curve a was obtained by using all terms in the equation. The drain voltage in either case was $V_D = 2.0$ V. The figure shows that eliminating the perturbation term reduces the potential along the depletion edge considerably. For instance, the change is about 70 percent at the drain end.

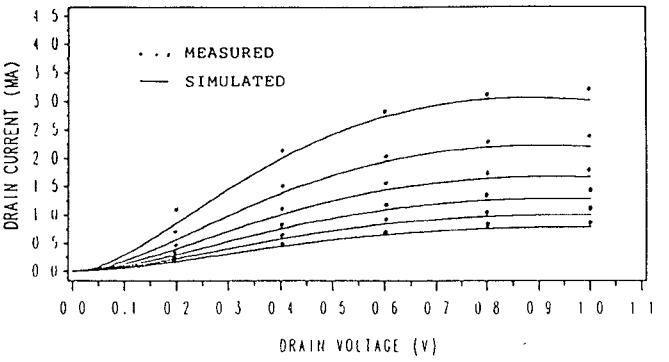

Fig. 3. Current–voltage characteristics for a GaAs MESFET with $L_g = 0.99$ μm.

IV. I–V Characteristics

The governing equation for the drain current, I_D, of GaAs MESFET's, assuming no generation and recombination of carriers in the channel, is given by

$$I_D = \iint J\,dS, \qquad J = qN_D\mu_n E. \tag{23}$$

Here, μ_n is the mobility and E is the electric field within the channel. Equation (23) also neglects any contribution due to Gunn domain formation. In the channel we use the value of E which exists at the depletion edge boundary C. This is justified as variations along the y axis are negligible. Using (19) we get

$$E = \left.\frac{\partial\phi}{\partial x}\right|_{C_0} = \sum_{n=0}^{\infty}\frac{(2n+1)\pi}{2h_s} \cdot \left[A_n\cosh\frac{(2n+1)\pi x}{2h_s} - B_n\cosh\frac{(2n+1)\pi(L_g - x)}{2h_s}\right] + \lambda\sum_{n=0}^{\infty}\left[\frac{(2n+1)\pi C_n}{2h_s}\sinh\frac{(2n+1)\pi h_s}{L_g}\cos\frac{\pi(2n+1)x}{L_g}\right]. \tag{24}$$

Substituting (24) into (23) yields

$$I_D = \{qN_D\mu_n\}\left\{\lambda\sum_{n=0}^{\infty}\frac{(2n+1)\pi}{2h_s}\int_{a-h_s}^{a-h_d}\int_0^W \cdot\left[C_n\sinh\frac{(2n+1)\pi h_s}{L_g}\cos\frac{\pi(2n+1)x}{L_g}\right]dz\,dh(x) + \sum_{n=0}^{\infty}\frac{(2n+1)\pi}{2h_s}\int_{a-h_s}^{a-h_d}\int_0^W\left[A_n\cosh\frac{(2n+1)\pi x}{2h_s} - B_n\cosh\frac{(2n+1)\pi(L_g - x)}{2h_g}\right]dz\,dh(x)\right\}. \tag{25}$$

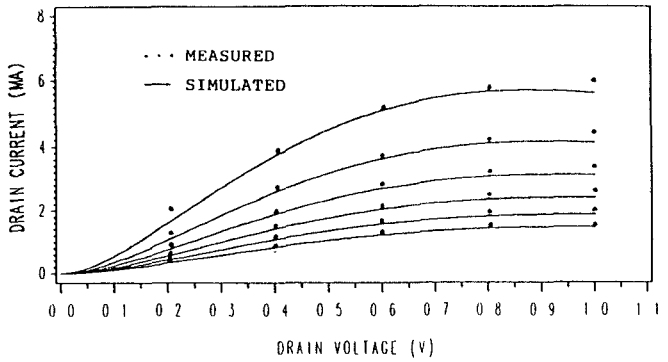

Fig 4. Current–voltage characteristics for a GaAs MESFET with $L_g = 0.53$ μm.

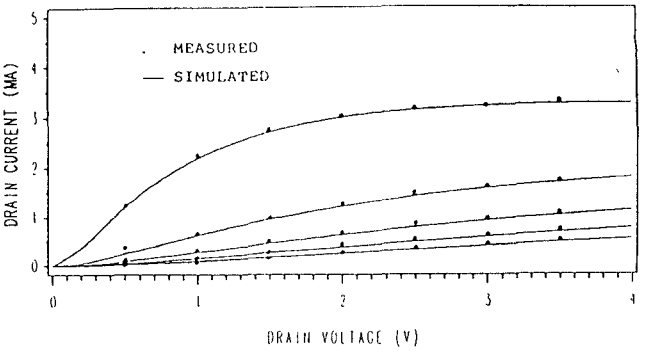

Fig 5. Current–voltage characteristics for a GaAs MESFET with $L_g = 0.21$ μm.

A linear approximation to $h(x)$ is

$$h(x) = \frac{h_d - h_s}{L_g} X - h_s \qquad h_d = a\sqrt{\frac{V_D + V_{bi} + V_g}{V_p}}$$

$$h_s = a\sqrt{\frac{V_{bi} + V_g}{V_p}}. \tag{26}$$

Substituting (26) into (25) and integrating gives

$$I_D = \frac{qN_D\mu_s W_a}{L_g}\left[\sqrt{\frac{V_D + V_{bi} + V_g}{V_p}} - \sqrt{\frac{V_{bi} + V_g}{V_p}}\right] \cdot \sum_{n=0}^{\infty} \frac{4V_p}{(2n+1)\pi} \cdot \left[\frac{V_D}{V_p} - \frac{2}{\pi^2(2n+1)^2}\sqrt{\frac{V_{bi} + V_g}{V_p}} \cdot \left\{\sqrt{\frac{V_D + V_{bi} + V_g}{V_p}} - \sqrt{\frac{V_{bi} + V_g}{V_p}}\right\}\right]. \tag{27}$$

Numerically simulated current–voltage characteristics using (27) are compared with experimentally determined results [12], [16] for submicron GaAs MESFET's with gate lengths of 0.99 μm, 0.53 μm, and 0.21 μm, as shown in Figs. 3, 4, and 5. The data used in the simulation were obtained from [12] and [16] and the expression used for the field-dependent mobility is due to Fair [10].

V. Discussion

The two-dimensional analytical MESFET models reported in the literature solve the Poisson equation using rectangular boundary conditions in the depletion region. The perturbation method allows one to obtain the potential distribution in a nonrectangular box which approximates the true boundary conditions. This results in the derivation of an $I-V$ equation which not only holds good in the subthreshold region of submicron devices but also is applicable in the linear and saturation regimes. Figs. 3–5 show an agreement of over 95 percent between the theoretical and the measured $I-V$ characteristics in the saturation regime. This agreement is lower for the linear portion of the $I-V$ characteristics. The deviation in the linear region is due in part to the limitations in the empirical expression used for the field-dependent mobility. Work is in progress to incorporate our earlier work on hot electron transport, such as velocity overshoot [15] effects, to model the $I-V$ equation.

Acknowledgment

The authors wish to thank Prof. R. Bansal for his valuable discussion and comments during the course of this study.

References

[1] P. C. Chao, P. M. Smith, S. Wanugu, W. Perkins, and E. D. Wolf, "Channel-length effects in quarter-micrometer gate-length GaAs MESFET's," *IEEE Electron Device Lett.*, vol. EDL-4, pp. 326–328, 1983.

[2] B. J. Zeghbroeck, W. Patrick, H. Meier, and P. Vettiger, "Submicrometer GaAs MESFET with shallow channel and very high transconductance," *IEEE Electron Device Lett.*, vol. EDL-8, pp. 118–120, March 1987.

[3] S. M. Sze, *Physics of Semiconductor Devices*, 2nd ed. New York: Wiley, ch. 6

[4] D. P. Kennedy and R. R. O'Brien, "Computer-aided two-dimensional analysis of the junction field-effect transistor," *IBM J. Res. Develop.*, vol. 14, pp. 95–116, 1970.

[5] H. L. Grubin and T. M. McHugh, "Hot electron transport effects in field-effect transistors," *Solid-State Electron.*, vol. 21, pp. 69–73, 1978.

[6] W. Shockley, "A unipolar field-effect transistors," *Proc. IRE*, pp. 1365–1367, 1952.

[7] G. C. Dacey and I. M. Ross, "The field-effect transistor," *Bell Syst. Tech. J.*, vol. 34, pp. 1149–1189, 1955.

[8] R. Pucel, H. Haus, and H. Statz, "Signal and noise properties of gallium arsenide microwave field-effect transistors," in *Advances in Electronics and Electron Physics*, vol. 38. New York: Academic Press, 1975, pp. 195–203

[9] K. Yamaguchi and H. Kodera, "Drain conductance of junction gate FETs in the hot electron range," *IEEE Trans. Electron Devices*, vol. ED-23, pp. 545–552, 1976

[10] R. B. Fair, "Graphical design and iterative analysis of the dc parameters of GaAs FET's," *IEEE Trans. Electron Devices*, vol. ED-21, pp. 357–362, 1974.

[11] J. D. Marshall and J. D. Meindl, "An analytical two-dimensional model for silicon MESFET's," *IEEE Trans. Electron Devices*, vol. 35, pp. 373–383, 1988

[12] Y. Kimiyoshi and H. Masahiro, "Determination of effective velocity saturation in n+ self-aligned GaAs MESFET's with submicron gate lengths," *IEEE Trans. Electron Devices*, vol. ED-33, pp. 1427–1432, 1986.

[13] G. F. Carrier and C. E. Pearson, *Partial Differential Equations* New York: Academic Press, 1988, ch. 8

[14] E. Donkor, "Design and modeling of submicron GaAs FETs," Ph.d. thesis, Univ. of Conn., 1988.

[15] E. Donkor and F. Jain, "Modeling of hot electron transport in GaAs and Si under transient and steady state conditions," *Bull. Amer. Phys. Soc.*, vol. 32, p. 1020, 1987

[16] W. Patrick, W. S. Mackie, S. P. Beaumont, C. D. W. Wilkinson, and C. H. Oxley, "Very short gate-length GaAs MESFETs," *IEEE Electron Device Lett.*, vol. EDL-6, pp. 471–472, 1985.